Pergamon

Int. J. Heat Mass Transfer. Vol. 41, Nos 4–5, pp. 699–707, 1998

Printed in Great Britain
0017–9310/98 $19.00+0.00

PII: S017–9310(97)00212–3

Flame cooling by a curved burner wall

R. M. M. MALLENS and L. P. H. DE GOEY†

Eindhoven University of Technology, Faculty of Mechanical Engineering (WOC), PO Box 513, 5600 MB Eindhoven, The Netherlands

(*Received* 18 *March* 1997 *and in final form* 20 *June* 1997)

Abstract—A recent investigation of flash-back of flames on slit and cylindrical burners showed that there is a systematic difference of about 10% between flash-back gradients of flames on slit and cylindrical burners with a burner diameter/width of 3.8 mm. In addition, the critical gradients become almost equal for burners with a diameter/width larger than about 6 mm. In this paper the effect of the burner wall curvature on the behaviour of, for example, the temperature field and the stand-off distance is analysed. The analysis shows that the burner wall curvature has an effect on the quenching layer thickness near the burner wall for burners smaller than about 6 mm. When the decrease of the cylindrical stand-off distance with increasing burner size is used to calculate the critical flash-back gradient based on a linear velocity profile for the cylindrical burners, the critical gradients for cylindrical and slit burners become almost the same for burners larger than about 5 mm. The analysis shows that the differences between flames on cylindrical and slit burners near the flash-back limit are mainly caused by differences in conductive heat transfer towards the burner wall, induced by burner wall curvature. © 1997 Elsevier Science Ltd.

1. INTRODUCTION

The stabilization of flames on a burner near the quenching or flash-back limit is generally believed to be dominated by heat loss of the flame to the burner wall. The amount of heat transported to the burner wall (mainly by conduction) depends on several factors, such as the distance of the flame above the burner, the temperature of the wall and the curvature of the burner wall. Cooling of the flame by the burner wall is especially important when studying phenomena in which the flame is very close to the burner wall, such as near the flash-back limit.

Flash-back of flames on cylindrical burners has been investigated by Lewis and von Elbe [1] and Harris *et al.* [2]. The investigation by Lewis and von Elbe [1] incorporates the effect of the burner diameter (ranging from 3.8 to 15.5 mm) on the critical flash-back gradient of natural gas/air flames. The critical gradient, defined as the velocity gradient at the wall when the flame flashes back, decreases for burner diameters larger than 4 mm. This decrease is attributed to the decreasing curvature of the parabolic velocity profile near the burner wall [1]. Harris *et al.* [2] investigated flash-back of methane/air flames on cylindrical burners with a diameter larger than 9 mm.

In a recent numerical and experimental study of flash-back of flames on slit and cylindrical burners [3] it is shown that there is a systematic difference of about 10% between flash-back gradients of flames on slit and cylindrical burners with a burner diameter/width $2R_0$ of 3.8 mm. A possible difference between the small cylindrical and slit burners is the enhanced cooling effect of the cylindrical burners which might influence the critical flash-back gradient. The investigation also showed that the critical flash-back gradients g_f for cylindrical and slit burners differ less than about 5% for burner widths/diameters larger than about 6 mm. This difference is not significant anymore because the flash-back gradient is determined numerically by reducing the velocity with 5% reduction steps. Smaller reduction steps are not useful because of model uncertainties, such as the predicted burning velocity by the chemical mechanism. The flash-back gradients measured and calculated by Mallens and de Goey [3] are given in Fig. 1(a). Further investigation of the effect of burner wall curvature on flame cooling and flash-back is necessary to ascertain whether the curvature of the burner wall can explain the differences.

Figure 1(b) shows the critical gradients after correction for the curvature of the parabolic velocity profile which is mainly held responsible [1] for the decrease of g_f with increasing burner size. The gradient $g_{f,lin}$, based on a linear velocity profile, is given by [3]

$$g_{f,lin} = \frac{2R_0 - \delta_q}{2R_0} g_f \tag{1}$$

with δ_q the quenching distance, for which we use a fixed value, being half the quenching diameter or width of cylindrical and slit burners [2]. Note that g_f is equivalent to the critical gradients reported in refs [1, 2]. The velocity v in the attachment point (at a distance δ_q from the burner wall) must equal the burning velocity S_L. This means that the gradient of a

† Author to whom correspondence should be addressed.

NOMENCLATURE

A	reaction parameter $[(\text{kg m}^{-3})^{1-\alpha-\beta}]$
c_p	specific heat [J kg^{-1} K^{-1}]
g_f	critical flash-back gradient of the velocity profile at the wall [s^{-1}]
J_i	Shvab-Zel'dovich variable for species i
L	length scale [m]
Le_i	Lewis number of species i
P	pressure [N m^{-2}]
R_g	specific gas constant [J kg^{-1} K^{-1}]
s_i	the mass of species i consumed per unit mass fuel [kg$_i$ kg$_{fu}^{-1}$]
T	temperature [K]
T_a	reaction rate parameter [K]
v_r	velocity in r-direction [m s^{-1}]
v_x	velocity in x-direction [m s^{-1}]
v_z	velocity in z-direction [m s^{-1}]
R_0	radius of curvature of the burner wall [m]
ΔH	reaction enthalpy [J kg$_{fu}^{-1}$]
Q_r	cooling rate by the burner wall [W]
Q_w	energy loss at the burner outflow [W]
S_L	flame speed [m s^{-1}]
Y_i	mass fraction of species i.

Greek symbols

α	reaction rate parameter
β	reaction rate parameter
δ_q	thickness of the quenching layer [m]
η	length scale [m]
λ	thermal conductivity [J m^{-1} K^{-1} s^{-1}]
$\dot{\rho}_{fu}$	fuel mass consumption rate [kg m^{-3} s^{-1}]
ρ	mixture density [kg m^{-3}].

Subscripts

cyl	referring to a cylindrical burner
car	referring to a slit burner
fu	fuel
ox	oxygen.

Superscripts

u	unburnt conditions
b	burnt conditions.

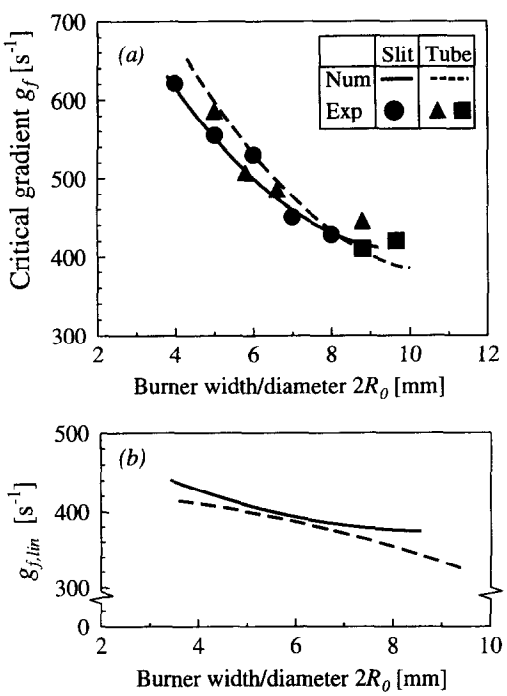

Fig. 1. Flash-back gradients g_f (a) and flash-back gradients based on a linear velocity profile $g_{f,lin}$ (b) for slit burners and cylindrical burners as a function of $2R_0$. The lines denote the numerical results for slit (solid line) and cylindrical burners (dotted line). The markers refer to experimental results obtained by Mallens and de Goey [3] (solid spheres and triangles) and Harris *et al.* [2] (solid squares).

linear velocity profile at the burner wall is given by $g_{f,lin} = S_L/\delta_q$ [3]. The burning velocity in the attachment point is close to its adiabatic value for both slit and tube burners [1]. The differences in $g_{f,lin}$ for slit and tube burners are, therefore, mainly determined by differences in δ_q.

The gradients based on a linear velocity profile in Fig. 1(b), however, still show a decreasing trend with R_0. This might be caused by other effects on the critical gradient, such as different velocities in the quenching layer near flash-back. The larger variation of $g_{f,lin}$ for the cylindrical burners might be caused by a decrease of δ_q with increasing R_0. In Fig. 1(b), however, δ_q is assumed to be constant.

In this paper we present an analysis of the differences between slit and cylindrical burners with respect to the cooling rate of the burner. The main goal of the analysis is to provide explanations for and to sustain the differences between the flash-back gradients of flames on slit and cylindrical burners [3] by analysing differences in δ_q between cylindrical and slit burners. The results of the analysis will also be used to investigate the effects of the burner size on the thickness of the quenching layer and the critical gradient.

The analysis is an extension of the analytical treatment performed by de Goey and de Lange [4] for slit burners. The extension basically consists of the introduction of a burner wall with a curvature $1/R_0$ and of the use of cylindrical coordinates (r, z) instead of Cartesian coordinates. The effect of the assumption

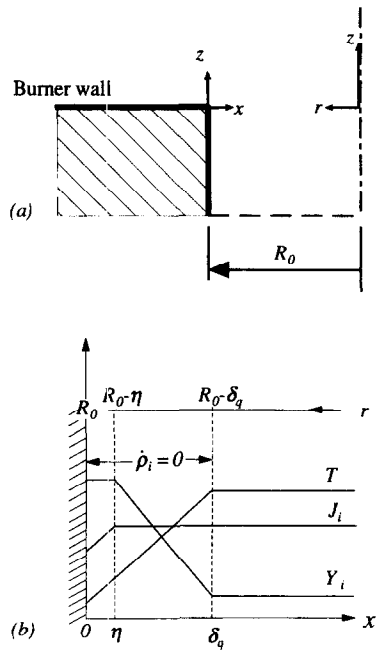

Fig. 2. The burner geometry with the two coordinate systems (a) and the schematical profiles of T, Y_i and J_i as a function of x (b).

of a constant thermal conductivity, a constant unidirectional velocity and the separation into two regions introduced in the analysis (see Section 2) on the behaviour of the temperature and the mass fractions in the quenching layer has been investigated [4] by modelling the situation depicted in Fig. 2(a) numerically (without the division of the domain in two regions). It was shown that the general behaviour of the temperature and the mass fractions in the quenching layer and the quenching layer thickness are not significantly affected by the assumptions mentioned above. Basic issues of the model are discussed in Section 2. The solutions for the temperature T, the mass fractions Y_i and the Shvab-Zel'dovich variables are presented in Sections 3, 4 and 5, respectively. In Section 6 the energy balance is verified. Then the effect of the burner wall curvature on the thickness of the quenching layer will be investigated (Section 7) and the behaviour of T and the fuel mass fraction Y_{fu} in the quenching layer is discussed (Section 8). Finally, in Section 9 the results of the analysis will be used to provide further explanations for the differences between critical flash-back gradients of flames on slit and cylindrical burners.

2. TWO-DIMENSIONAL MODEL

The burner geometry is the same as the geometry used in ref. [4] [see Fig. 2(a)]. The only difference is that the burner wall has a non-zero curvature $1/R_0$. Two coordinate systems are given in Fig. 2(a). One system (x, z) that we used by de Goey and de Lange [4] and the (r, z) system that will be used in the present study. The coordinate system (x, z) is given because the results will be compared with the results obtained in ref. [4]. We will now introduce the basic assumptions. It is assumed that there is no lateral velocity component ($v_r = v_x = 0$). Note that this assumption reduces the continuity equation to $\rho v_z = \rho^u v_z^u$, where the superscripts u refer to the conditions at in the unburnt mixture $z \to -\infty$. The ideal gas law ($P = \rho R_g T$) is used as the equation of state, where P is the pressure and R_g the specific gas constant of the mixture. The deflagration process considered here is a low Mach number flow which implies that the pressure can be assumed to be constant. Furthermore, the constant R_g is assumed to be independent of the mixture composition. These assumptions lead to a density which depends on temperature only: $\rho T = \rho^u T^u$.

The thermal conductivity λ and the specific heat c_p are both taken to be constant. For the Lewis numbers of fuel and oxygen we use $Le_i = 1$. These assumptions are introduced to make the analytical treatment possible.

As chemical model a one-step irreversible reaction fuel + oxygen → products is used with an Arrhenius-type source term [5]. The source term for the fuel mass fraction equation $\dot{\rho}_{fu}$ is given by

$$\dot{\rho}_{fu} = -A\rho^{(\alpha+\beta)} Y_{fu}^{\alpha} Y_{ox}^{\beta} e^{(-T_a/T)}. \tag{2}$$

The reaction rate parameters A, α, β and T_a are determined by fitting the burning velocity S_L as a function of equivalence ratio ϕ and flame temperature T_b to experimental results [6–8]. This chemical model is also used in the earlier mentioned study of flash-back [3]. The conservation for the temperature T and mass fraction of species i, Y_i with i = (fu)el, (ox)ygen, (pr)oducts, now become

$$\frac{1}{L}\frac{\partial T}{\partial z} - \frac{\partial^2 T}{\partial z^2} - \frac{1}{r}\frac{\partial}{\partial r}\left(r\frac{\partial T}{\partial r}\right) = -\Delta H \dot{\rho}_{fu} \tag{3}$$

and

$$\frac{1}{\lambda}\frac{\partial Y_i}{\partial z} - \frac{\partial^2 Y_i}{\partial z^2} - \frac{1}{r}\frac{\partial}{\partial r}\left(r\frac{\partial Y_i}{\partial r}\right) = s_i \dot{\rho}_{fu} \tag{4}$$

with ΔH the combustion enthalpy and s_i the stoichiometric factor of species i. The values of the physical parameters, such as λ, c_p, ΔH and the unburnt and burnt values of T and Y_{fu}, are given in Table 1. The equivalence ratio ϕ is equal to one. The length scale L is defined by

$$L = \frac{\lambda}{\rho^u v_z^u c_p}. \tag{5}$$

In the remainder of this section the behaviour of T and Y_i in the quenching layer will be discussed to clarify some additional assumptions in the analysis. Profiles of the Shvab-Zel'dovich variable

$$J_{fu,ox} = \frac{c_p T}{\Delta H} + \frac{Y_{fu,ox}}{s_{fu,ox}} \tag{6}$$

Table 1. The physical parameters and the temperature and mass fractions of fuel in the burnt and the unburnt mixture

Parameter	Value	Dimension
ρ_u	1.13	[kg m^{-3}]
T_u	300	[K]
T_b	2250	[K]
Y_{fu}^u	0.055	[—]
Y_{fu}^b	0.0	[—]
λ	0.092	[J m^{-1} K^{-1} s^{-1}]
c_p	1365	[J/kg^{-1} K^{-1}]
ΔH	4.813×10^7	[J kg^{-1}]
s_{ox}	3.883	[kg$_{ox}$ kg$_{fu}^{-1}$]
A	2.6×10^{15}	[(kg m^{-3})$^{(1-\alpha-\beta)}$]
α	1.2	
β	2.8	
T_a	16900	[K]

will be treated as well. Physically, J_i can be interpreted as the sum of thermal enthalpy $\equiv c_pT$ and chemical enthalpy $\equiv \Delta H\ Y_i/s_i$ in the mixture. The expression for J_i can be derived from a linear combination of the conservation equations for T and Y_i. The source terms of T and Y_i cancel out if $Le_i = 1$. Note that this implies that J_i is not affected by the chemical source term in the flame.

We assume that the flame is flat near the stabilization point (parallel to the r-axis) and that the flame flashes back if the velocity v_z^u is decreased. This implies that the cooling near the burner wall and the quenching distance δ_q are maximal. The flat flame is assumed to be stabilized at $z = 0$ for $r < R_0-\delta_q$ and is extinguished due to the cooling rate by the burner wall for $R_0-\delta_q < r < R_0$. This implies that the fuel mass consumption rate $\dot\rho_{fu}$ is almost zero in the latter area [see Fig. 2(b)]. We will, therefore, assume that $\dot\rho_{fu} = 0$ for $R_0+\delta_q < r < R_0$. The zero fuel mass consumption implies that the mass fractions only change due to diffusion and convection. This, in turn, leads to constant mass fractions in a thin layer of thickness η at the wall ($R_0-\eta < r < R_0$) because there is no diffusion flux through the wall. The Shvab-Zel'dovich variables J_i are not affected by the presence of the flame because the differential equation for J_i has no chemical source term. This implies that J_i is not influenced by the presence of the flame at $r = R_0-\delta_q$. This, and the fact that J_i is constant in the flame region, implies that J_i is constant in a region $R_0-\delta_q < r < R_0-\eta$. Because of the fact that J_i is not affected by the chemical source term in the flame, the decrease of the mass fractions has to be proportional to the increase of T in such a way that J_i is constant; i.e. the diffusion of heat (c_pT) towards the wall is compensated by a chemical enthalpy flux of $\Delta H\ Y_i/s_i$ caused by diffusion of fuel and oxygen. The Shvab-Zel'dovich variables will decrease for $R_0-\eta < r < R_0$ because the diffusion of fuel and oxygen is zero in this area [see Fig. 2(b)].

3. THE THERMAL BOUNDARY LAYER

In this section an approximate solution of the energy equation for the temperature will be presented. The domain is divided into two regions: a region $R_0-\delta_q < r < R_0$ where the cooling is important and a region $r < R_0-\delta_q$ in which the profiles of Y_i, T and J_i are independent of the distance from the burner wall. The temperature profile as a function of z for $r < R_0-\delta_q$ is given by the solution of a flat flame independent of r:

$$T(r,z) = T^u + \Delta T e^{z/L} \quad \text{for } r < R_0-\delta_q,\ z \leqslant 0$$

$$T(r,z) = T^b \quad \text{for } z > 0.$$

This means that the reaction sheet at $z = 0$ is considered to be indefinitely thin [9]. $\Delta T = T_b - T_u$ denotes the difference between the flame and the unburnt temperature. The boundary conditions for the area $R_0-\delta_q \leqslant r \leqslant R_0$ where cooling is important then becomes

$$z \leqslant 0;\quad r = R_0:\quad T = T^u$$

$$z \leqslant 0;\quad r = R_0-\delta_q:\quad T \to T^u + \Delta T e^{z/L}$$

and:

$$z \to -\infty;\quad R_0-\delta_q \leqslant r \leqslant R_0:\quad T = T^u.$$

The fuel mass consumption rate $\dot\rho_{fu}$ is assumed to be zero in the cooling layer. This assumption, the shape of the boundary conditions and the assumption of a unidirectional flow imply that a separation of directions may be applied. This leads to the trial solution:

$$T(r,z) = T^u + t_1(z)\cdot t_2(r). \tag{7}$$

The separation of directions makes it possible to give an exact solution of the energy solution for the given boundary conditions. Substitution of eqn (7) into the energy eqn (3) with $\dot\rho_{fu} = 0$ gives

$$\frac{1}{t_1}\left[\frac{1}{L}\frac{\partial t_1}{\partial z} - \frac{\partial^2 t_1}{\partial z^2}\right] = \frac{1}{rt_2}\frac{\partial}{\partial r}\left(r\frac{\partial t_2}{\partial r}\right) = c^2 \tag{8}$$

with c^2 the separation constant. Note that L is assumed constant in eqns (3) and (8), which implies that the solution given below is restricted to a constant v_z in the r-direction. Two different solution types for $t(z)$ and $t_2(r)$ are taken into account:

$$\text{for } c^2 = 0:\quad t_1 = k_1 e^{\Gamma\pm z};\quad t_2 = k_2\ln(r) + k_3 \tag{9}$$

and

$$\text{for } c^2 > 0:\quad t_1 = k_4 e^{\Gamma\pm z};\quad t_2 = k_5 I_0(cr) + k_6 K_0(cr) \tag{10}$$

with $\Gamma_\pm = 1/2L[1\pm\sqrt{1-(2cL)^2}]$. The functions $I_0(cr)$ and $K_0(cr)$ are modified Bessel functions of zeroth order. The $c^2 < 0$ solution type is not taken into account because it shows an oscillatory behaviour

which is not in accordance with the flat flame solution for $r < R_0+\delta_q$ and the solutions for $c^2 \geqslant 0$ are sufficient to describe the desired solution. Note that the solution given above also hold for the mass fractions and the Shvab-Zel'dovich variables as long as they are described by the same type of conservation equations.

The solution given by eqn (9) for $c^2 = 0$ satisfies all the boundary conditions for the energy eqn (3):

$$T(r,z) = T^u + \Delta T \frac{\ln\left(\frac{r}{R_0}\right)}{\ln\left(1-\frac{\delta_q}{R_0}\right)} e^{z/L}$$

$$\text{for } R_0-\delta_q < r < R_0. \quad (11)$$

The solution found for a burner wall with no curvature ($1/R_0 = 0$) by de Goey and de Lange [4] should be recovered if the limit for $R_0 \to \infty$ is taken in eqn (11). The solution found in ref. [4] reads

$$T(x,z) = T^u + \Delta \frac{x}{\delta_q} e^{z/L}. \quad (12)$$

When $r = R_0 - x$ is substituted into eqn (11), it can be shown that eqns (11) and (12) become equal for $R_0 \to \infty$ by using the expansion $\ln(1+\varepsilon) = \varepsilon + \mathcal{O}(\varepsilon^2)$ for $\varepsilon \to 0$.

The resulting profiles $T(r, z = 0)$ are shown in Fig. 3 for different values of R_0. The effect of R_0 on the behaviour of the temperature in the quenching layer will be discussed after the section in which the thickness of the thermal boundary layer is discussed.

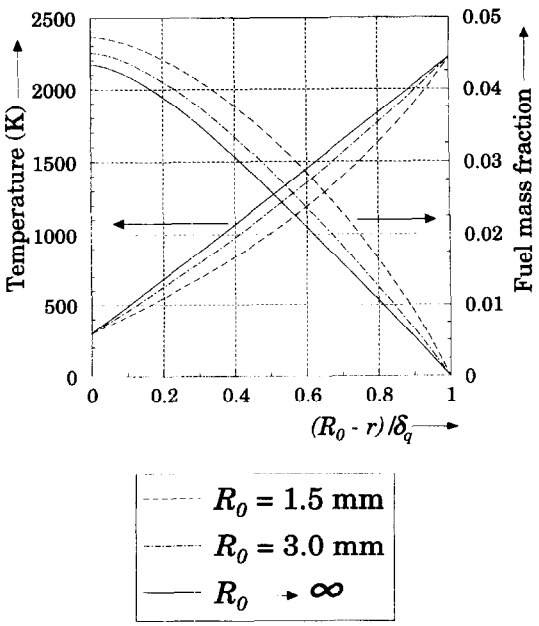

Fig. 3. The profiles of T and Y_{fu} for various values of R_0. The horizontal distance from the wall is normalized with the quenching distance.

4. THE DIFFUSIVE BOUNDARY LAYER

The mass fractions of fuel and oxygen are described by the same type of differential equation as the temperature T. This means that the solutions given in eqns (9) and (10) are also valid for Y_i. The boundary conditions for Y_i are:

$$z \leqslant 0; \quad r = R_0: \quad \frac{\partial Y_i}{\partial r} = 0$$

$$z \leqslant 0; \quad r = R_0-\delta_q: \quad Y_i \to Y_i^u + \Delta Y_i e^{z/L}$$

$$z \to -\infty; \quad R_0-\delta_q \leqslant r: \quad Y_i = Y_i^u$$

with ΔY_i equal to $Y_i^u - Y_i(R_0-\delta_q, 0)$ (ΔY_i will be calculated later in the text). Note that the boundary condition at $r = R_0$ is of a different type than the boundary condition for T. This implies that a solution analogous to eqn (11) is not sufficient to describe the solution for Y_i near the burner wall. The correct shape of the mass fraction profiles is found by the addition of $c^2 > 0$ solutions to the $c^2 = 0$ solution. The inclusion of the $c^2 = 0$ solution is necessary to ensure that the Shvab-Zel'dovich variables are not influenced by the presence of the flame at $r = R_0-\delta_q$. The solution for Y_i is, therefore, given by

$$Y_i(r,z) = Y_i^u + \frac{\Delta Y_i}{\ln\left(1-\frac{\delta_q}{R_0}\right)}\left[\ln\left(\frac{r}{R_0}\right)e^{z/L} + \tilde{Y}_i(r,z)\right] \quad (13)$$

with

$$\tilde{Y}_i(r,z) = \int_0^\infty I_0(cr)\left[\mathcal{F}(c)\exp\left(\frac{z}{2L}[1+\sqrt{1-4c^2L^2}]\right) + \mathcal{G}(c)\exp\left(\frac{z}{2L}[1-\sqrt{1-4c^2L^2}]\right)\right]dc. \quad (14)$$

The modified Bessel function $K_0(cr)$ is not included in equation (14) because $K_0(cr)$ decreases with increasing cr while $\tilde{Y}_i(r,z)$ should be increased with increasing r. The amplitudes $\mathcal{F}(c)$ and $\mathcal{G}(c)$ indicate the contribution of solutions with length scale $1/c$ in the r-direction. Note that solutions with $c < 0$ do not contribute because $I_0(cr)$ is symmetrical around $cr = 0$. The procedure for obtaining expressions for $\mathcal{F}(c)$ and $\mathcal{G}(c)$ is similar to the procedure used in ref. [4] and will not be repeated here. The resulting expression for $\tilde{Y}(r,z)$ reads

$$\tilde{Y}_i(r,z) = -\frac{1}{R_0}\frac{2L}{\pi}\int_0^\infty dk \frac{I_0\left(\frac{\sqrt{1+k^2}}{2L}r\right)}{I_1\left(\frac{\sqrt{1+k^2}}{2L}R_0\right)} \times \left[\frac{1}{\sqrt{1+k^2}}\right]^3 \cos\left(k\frac{z}{2L}\right)e^{-(z/2L)} \quad (15)$$

with $ik \equiv \sqrt{1-4c^2L^2}$. ΔY_i can be calculated by setting Y_i equal to the burnt value Y_i^b in the flame attachment point $(r,z)=(R_0-\delta_q,0)$. Note that the expression for $\tilde{Y}_i$ is derived from solutions restricted to a constant velocity in the r-direction which implies that the following expression for ΔY_i is also limited to this special case. This leads to the following expression for ΔY_i:

$$\Delta Y_i = \frac{(Y_i^b - Y_i^u)\ln\left(1-\frac{\delta_q}{R_0}\right)}{\ln\left(1-\frac{\delta_q}{R_0}\right)+\tilde{Y}_i(R_0-\delta_q,0)}. \quad (16)$$

A similar expression for ΔT is derived in the following section. The above solution is verified by calculating the limit for $R_0 \to \infty$. The Cartesian solution found in ref. [4] has to be recovered then. The solution [4] is equal to

$$Y_i(x,z) = Y_i^u + \Delta Y_i \delta_q \left[\frac{x}{\delta_q^2}e^{z/L} + \tilde{Y}_i(x,z)\right] \quad (17)$$

with

$$\tilde{Y}_i(x,z) = -\frac{1}{\delta_q}\frac{2L}{\pi}\int_0^\infty dk \exp\left(-\frac{\sqrt{1+k^2}}{2L}x\right) \times \left[\frac{1}{\sqrt{1+k^2}}\right]^3 \cos\left(\frac{kz}{2L}\right)e^{-(z/2L)}. \quad (18)$$

First note that the factor $1/R_0$ in eqn (15) together with the factor $1/\ln(1-\delta_q/R_0)$ becomes equal to the factor $1/\delta_q$ in eqn (18) for $R_0 \to \infty$. Furthermore, when $r = R_0 - x$ is substituted in eqn (13) it can be shown that eqn (13) becomes equal to eqn (17) for $R_0 \to \infty$ if

$$\lim_{R_0\to\infty}\left[\frac{I_0\left(\frac{\sqrt{1+k^2}}{2L}(R_0-x)\right)}{I_1\left(\frac{\sqrt{1+k^2}}{2L}R\right)}\right] = \exp\left(-\frac{\sqrt{1+k^2}}{2L}x\right) \quad (19)$$

which follows from the following property of a modified Bessel function of order v:

$$\lim_{z\to\infty} I_v(z) \propto \frac{e^z}{\sqrt{2\pi z}}. \quad (20)$$

The profiles of the mass fractions $Y_i(r, z=0)$ given by eqn (13) are also given in Fig. 3 for various values of R_0. They will be discussed after the section with the discussion of the thickness of the thermal boundary layer.

5. THE SOLUTION OF THE SHVAB-ZEL'DOVICH VARIABLES

The previous expression of ΔT in eqn (11) has to be reconsidered before we turn to the solution for the Shvab-Zel'dovich variables. This is necessary because the solution given in eqn (11) gives rise to a discontinuous derivative of $J_i(r,z)$ at $r = R_0-\delta_q$. The derivative becomes continuous if the decline of the mass fractions is proportional to the increase of T in the quenching layer. We will, therefore, redefine the solution for T as

$$T(r,z) = T^u + \Delta T \frac{\ln\left(\frac{r}{R_0}\right)}{\ln\left(1-\frac{\delta_q}{R_0}\right)}e^{z/L} \quad (21)$$

for $R_0-\delta_q < r < R_0$ and with ΔT defined as

$$\Delta T = \frac{(T^b - T^u)\ln\left(1-\frac{\delta_q}{R_0}\right)}{\ln\left(1-\frac{\delta_q}{R_0}\right)+\tilde{Y}_i(R_0-\delta_q,0)}. \quad (22)$$

The solution for J_i can be found by substitution of the solution for T and Y_i in eqn (6):

$$J_i(r,z) = J_i^u + \frac{\Delta Y_i}{s_i \ln\left(1-\frac{\delta_q}{R_0}\right)}\tilde{Y}_i(r,z). \quad (23)$$

Note that the solution given above approaches J_i^u for $r \to R_0-\delta_q$ which implies that the Shvab-Zel'dovich variables are indeed not influenced by the presence of the flame at $r = R_0-\delta_q$. Therefore, the use of eqn (22) in the solution of the energy equation leads to a physically correct behaviour of the Shvab-Zel'dovich variables and enhances the quality of the further results.

The solution for the Shvab-Zel'dovich variables for $z = 0$ is given in Fig. 4 for various values of R_0. The effect of the burner radius R_0 is negligible for $R_0 > 3$ mm. This indicates that the difference between cylindrical burners and slit burners (with respect to the behaviour of J_i) becomes negligible for burners with a diameter or width larger than 6 mm.

6. THE ENERGY BALANCE

The gross energy conservation in the region below the flame can be verified by using the solution for $J_i(r,z)$ and $T(r,z)$. The total cooling rate by the wall can be calculated by using eqn (11):

$$Q_w = 2\pi R_0 \int_{-\infty}^{0} dz\, \lambda \left.\frac{\partial T}{\partial r}\right|_{r=R_0}$$

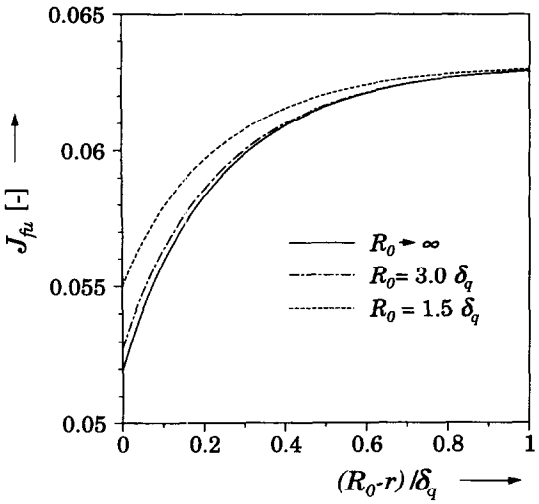

Fig. 4. The profiles of $J_{fu}(r, z = 0)$ for various values of R_0.

$$= 2\pi R_0 \int_{-\infty}^{0} \mathrm{d}z \frac{\mathrm{e}^{z/L}\lambda\Delta T}{R_0 \ln\left(1-\frac{\delta_q}{R_0}\right)} = \frac{2\pi\lambda\Delta TL}{\ln\left(1-\frac{\delta_q}{R_0}\right)}. \quad (24)$$

The total energy loss at the outflow of the tube ($z = 0$) can be calculated as follows:

$$Q_r = 2\pi\rho^u v^u \Delta H \int_0^{R_0} r\,\mathrm{d}r[J_i^u - J_i(r, z=0)]$$

$$= 2\pi\rho^u v_z^u \Delta H \int_0^{R_0} r\,\mathrm{d}r \frac{\Delta Y_i}{s_i \ln\left(1-\frac{\delta_q}{R_0}\right)} \tilde{Y}_i(r,0) \quad (25)$$

which, after substitution of eqn (15), becomes

$$Q_r = \frac{-4\pi\rho^u v_z^u \Delta H \Delta Y_i L}{s_i \pi R_0 \ln\left(1-\frac{\delta_q}{R_0}\right)} \int_0^{R_0} r\,\mathrm{d}r$$

$$\times \int_0^{\infty} \mathrm{d}k \frac{I_0\left(\frac{\sqrt{1+k^2}}{2L} r\right)}{I_1\left(\frac{\sqrt{1+k^2}}{2L} R_0\right)} \left[\frac{1}{\sqrt{1+k^2}}\right]^3. \quad (26)$$

The integral in the previous equation can be rewritten by substituting $\alpha = r/L$ and the constant $\alpha_0 = R_0/L$. Then the integral over the Bessel function I_0 can be calculated which results in a Bessel function I_1. Calculation of the integral over k then leads to the following expression for the heat loss at the burner outflow:

$$Q_r = \frac{2\pi\lambda\Delta TL}{\ln\left(1-\frac{\delta_q}{R_0}\right)} \quad (27)$$

where we used:

$$\frac{\Delta H \Delta Y_i}{s_i \delta_q} = \frac{c_p \Delta T}{\delta_q} \quad \text{and} \quad L = \frac{\lambda}{\rho^u v_z^u c_p}.$$

The fact that eqns (24) and (27) lead to the same result proves that the solutions for T, Y_i and J_i in the quenching layer satisfy energy conservation.

7. THE THICKNESS OF THE THERMAL BOUNDARY LAYER

In this section an estimate will be made of the effect of the burner wall curvature R_0 on the thickness of the thermal boundary layer δ_q. The estimate is based on the local balance of the burning velocity and the mixture velocity in the attachment point $(r, z) = (R_0 - \delta_q, 0)$ [4]. The solution for the Shvab-Zel'dovich variables indicates that the maximum temperature and burning velocity are only reached for $\delta_q \to \infty$. This means that δ_q has to be so large that the flame temperature and burning velocity in the attachment point are close to their maximum values (denoted by T_b and S_L). The temperature in the attachment point $(R_0 - \delta_q, 0)$ can be calculated from eqn (11). The result $(T(R_0-\delta_q) - T^u)/(T^b - T^u)$ is given in Fig. 5(a). The burning velocity in the attachment point $S_L(R_0-\delta_q, 0)$ [see Fig. 5(b)] is calculated using the analytical relation between the burning velocity and the flame temperature for a flat burner-stabilized flame [4, 10]:

$$\ln\left(\frac{S_L(R_0-\delta_q, 0)}{S_L}\right) = \frac{-T_a}{2T(R_0-\delta_q, 0)} + \frac{T_a}{2T_b} + \frac{\alpha+\beta+2}{2} \ln\left(\frac{T(R_0-\delta_q, 0)}{R_b}\right). \quad (28)$$

The burning velocity in the attachment point pre-

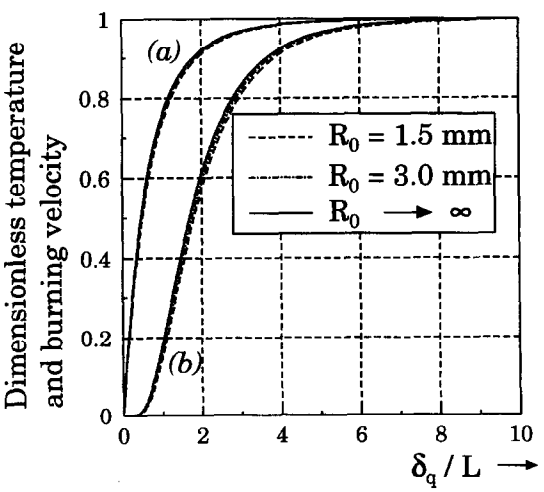

Fig. 5. The temperature $(T(R_0-\delta_q) - T^u)/(T^b - T^u)$ (a) and the burning velocity $S_L(R_0-\delta_q, 0)/S_L$ (b) in attachment point $(R_0-\delta_q, 0)$ for various values of R_0.

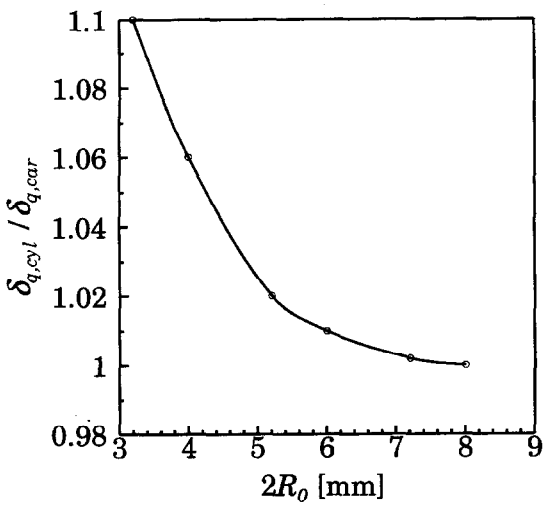

Fig. 6. The ratio of the stand-off distances of the flames on the cylindrical burners and the slit burner ($\delta_{q,cyl}/\delta_{q,car}$) as a function of R_0 predicted by the analytical model.

dicted by eqn (28) is also given in Fig. 5 for three values of R_0. The estimated value for δ_q is approximately 0.85 mm when the stabilization criterion $S_L(R_0-\delta_q,0)/S_L = 0.98$ for slit burners ($R_0 \to \infty$) is taken. This estimation can also be made by using the same criterion for other values of R_0. In this way, the ratio of the stand-off distances for cylindrical burners $\delta_{q,cyl}$ and the slit burner $\delta_{q,car}$ can be calculated. Variation of the value for the criterion $S_L(R_0-\delta_q,0)/S_L$ between 0.97 and 0.99 did not significantly affect the ratio $\delta_{q,cyl}/\delta_{q,car}$. The resulting ratio $\delta_{q,cyl}/\delta_{q,car}$ is plotted as a function of R_0 in Fig. 6. Note that this ratio only changes due to differences in conductive energy transport at different values of R_0 because the convective term in the energy eqn (3) is independent of R_0.

8. BEHAVIOUR OF T AND Y_{fu} IN THE QUENCHING LAYER

The profiles for T and Y_{fu} in the quenching layer at $z = 0$ are given in Fig. 3. Note that the horizontal distance in Fig. 3 is normalized with the quenching distance δ_q so that effects due to differences in the stand-off distance are not visible in Fig. 3. It is clearly visible in Fig. 3 that the temperature in the quenching layer decreases for smaller cylindrical burners due to the enhanced cooling by these burners. The decreasing temperature leads to higher fuel mass fractions in the quenching layer because of the conservation of J_{fu} for $r < (R_0-\eta)$. The profiles of T and Y_{fu} for the cylindrical burners almost coincide with the profiles for the slit burner ($R_0 \to \infty$) for burner radii larger than approximately 3 mm, which is in agreement with the behaviour of δ_q discussed in the previous section.

The heat loss of the flame in the attachment point for $r = R_0-\delta_q$ and $y = 0$ can be determined from

$$Q_{flame} = \lambda \left.\frac{\partial T}{\partial r}\right|_{r=R_0-\delta_q;y=0} = \frac{\lambda \Delta T}{(R_0-\delta_q)\ln\left(1-\dfrac{\delta_q}{R_0}\right)}. \quad (29)$$

Evaluation of eqn (29) in the attachment point $(R_0-\delta_q, 0)$ results in values of $3.4 \cdot 10^5$, $2.2 \cdot 10^5$ and $2.1 \cdot 10^5$ J m^{-2} s^{-1} for $R_0 = 1.5$, 3.0 and $R_0 \to \infty$, respectively. Note that the heat loss of the flame for $R_0 = 3.0$ mm differs 5% from the heat loss for $R_0 \to \infty$ which is comparable to the difference in the critical gradients for slit and cylindrical burners [see Fig. 1(b)].

9. THE DEPENDENCE OF FLASH-BACK GRADIENTS ON BURNER GEOMETRY AND SIZE

We will now examine the dependence of the critical flash-back gradient on burner geometry and size by using the results obtained for $\delta_{q,cyl}/\delta_{q,car}$ in the previous section.

It is clearly visible in Fig. 1(b) that $g_{f,lin}$ for the cylindrical burners shows a significantly larger variation with R_0 than the gradients for the slit burners. In addition, the cylindrical values for $g_{f,lin}$ do not appear to approach the slit burner values for larger burners. This is probably due to the constant value for $\delta_{q,cyl} = 1.6$ mm used in Fig. 1(b), while the analytical model predicts a decreasing stand-off distance $\delta_{q,cyl}$ with increasing R_0 (which is also expected from a physical point of view). This result will now be used to recalculate $g_{f,lin}$ for the cylindrical burners. The aim of this calculation is to investigate whether the larger variation of $g_{f,lin}$ for cylindrical burners and the observation that the gradients for large cylindrical and slit burner do not become equal are mainly caused by the assumption that $\delta_{q,cyl}$ is constant in Fig. 1(b). The absolute values of $\delta_{q,cyl} \approx 1.1$ mm for $R_0 = 1.6$ mm and $\delta_{q,car} \approx 0.97$ mm for $R_{d,car} = 1.6$ mm predicted by the analytical model, however, deviate about 20–30% from the experimental values $R_{d,cyl} = 1.6$ mm and $R_{d,car} = 1.2$ mm. The stand-off distance of the flames computed numerically is probably much closer to the experimental values $R_{d,cyl}$ and $R_{d,car}$. This can be concluded from the good reproduction of g_f by the numerical model. We, therefore, decided to use the experimental values $R_{d,cyl}$ and $R_{d,car}$ for $\delta_{q,cyl}$ and $\delta_{q,car}$ for $R_0 = 1.6$ mm. The decrease of $\delta_{q,cyl}/\delta_{q,car}$ is then used to calculate $\delta_{q,cyl}$ as a function of R_0. The stand-off distance $\delta_{q,car}$ is assumed to be constant and equal to $R_{d,car} = 1.2$ mm. The resulting values for $\delta_{q,car}$ and $\delta_{q,cyl}$ are substituted in eqn (1) to calculate $g_{f,lin}$. Note that $g_{f,lin} = S_L/\delta_q$ and that $g_{f,lin,car}/g_{f,lin,cyl} = \delta_{q,cyl}/\delta_{q,car}$.

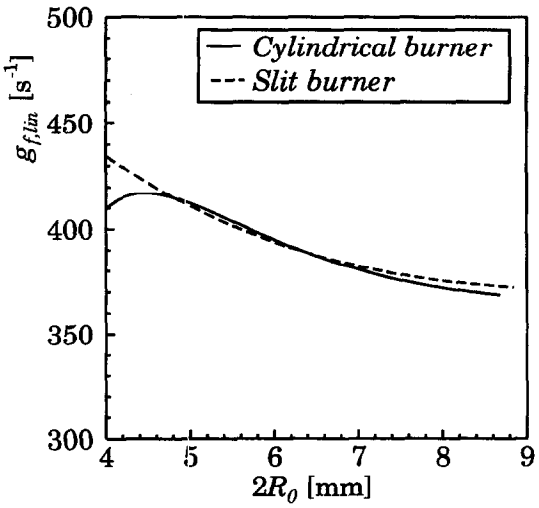

Fig. 7. The critical gradient based on a linear velocity profile [eqn (1)]. For the slit burners we used $\delta_q = 1.2$ [2]; for the cylindrical burners we used $\delta_q = 1.6$ mm [2] for $2R_0 = 3.2$ mm. For larger diameters δ_q is assumed to decrease according to $\delta_{q,cyl}/\delta_{q,car}$ given in Fig. 6.

The result for $g_{f,lin}$ is given in Fig. 7. The variation of $g_{f,lin}$ with burner size for cylindrical burners in Fig. 7 is almost equal to the variation for the slit burners. This illustrates that $g_{f,lin}$ becomes approximately equal for large slit and cylindrical burners if a decreasing value of $\delta_{q,cyl}$ is used. Only near $R_0 \approx 2$ mm is an increase detected, which is caused by the steep decrease of $g_{f,cyl}$ near the quenching diameter which, in turn, is caused by the large cooling rate near flame quenching (the flame quenches for $R_{d,cyl} = 1.6$ mm). Note that the critical gradient becomes zero for $R_0 = R_{d,cyl}$ (also see ref. [1]). For slit burners the gradient becomes zero at $R_{d,car} = 1.2$ mm. The behaviour of the cylindrical $g_{f,lin}$ as a function of R_0 is also physically more justified since it has the same behaviour as for slit burners for large values of $2R_0$.

10. CONCLUSIONS

An analysis has been presented to predict the effect of the burner wall curvature on the cooling rate by the burner. The analysis has been used to investigate the stand-off distance ratio of cylindrical and slit burners $\delta_{q,cyl}/\delta_{q,car}$ as a function of R_0. The results show that the differences in stand-off distance between cylindrical and slit burners increases to about 10% for a burner width/diameter of 4 mm. This is of the same order of magnitude as the observed differences between critical flash-back gradients based on a linear velocity profile of flames on slit and on cylindrical burners [3].

Furthermore, the analysis shows that the effect of the burner wall curvature on the profiles of T, Y_i and J_i is negligible for burners larger than about 6 mm. The study indicates that the observed differences in flash-back behaviour [3] are dominated by differences in conductive heat transfer to the burner wall due to burner wall curvature.

Acknowledgements—The support of Gastec N.V. and EnergieNed, The Netherlands, is gratefully acknowledged.

REFERENCES

1. Lewis, B. and von Elbe, B., Stability and structure of burner flames. *Journal of Chemistry and Physics*, 1943, **11**, 75–97.
2. Harris, M. E., Grumer, J., von Elbe, B. and Lewis, B., Burning velocities, quenching and stability data on nonturbulent flames of methane and propane with oxygen and nitrogen. In *Third Symposium on Combustion, Flame and Explosion Phenomena*, 1949 pp. 80–88.
3. Mallens, R. M. M. and de Goey, L. P. H., Flash-back of laminar methane/air flames. In *Proceedings of the Third Asian–Pacific Conference on Combustion and Energy Utilization*, Vol. II, 1995, pp. 644–649.
4. de Goey, L. P. H. and de Lange, H. C., Flame cooling by a burner wall. *International Journal of Heat and Mass Transfer*, 1994, **37**, 635–646.
5. de Lange, H. C. and de Goey, L. P. H., Two-dimensional methane/air flames. *Combustion Science and Technology*, 1993, **92**, 423–427.
6. Kaskan, W. E., The dependence of flame temperature on mass burning velocity. In *Sixth Symposium (International) on Combustion*. The Combustion Institute, Pittsburgh, PA, 1967, pp. 134–143.
7. Andrews, G. E. and Bradley, D., The burning velocity of methane–air mixtures. *Combustion and Flame*, 1972, **19**, 275–288.
8. van Maaren, A., Thung, D. S. and de Goey, L. P. H., Measurement of flame temperature and adiabatic burning velocity of methane/air mixtures. *Combustion Science and Technology*, 1994, **96**, 327–344.
9. Bush, W. B. and Fendell, F. E., *Combustion Science and Technology*, 1970, **1**, 421–428.
10. Williams, F. A., *Combustion Theory*, 2nd edn. Addison–Wesley, Reading, MA, 1988.